Northumbria Research Link

Northumbria University
NEWCASTLE

UniversityLibrary

Accepted Manuscript

Title: Enhanced NH$_3$ gas-sensing performance of silica modified CeO$_2$ nanostructure based sensors

Authors: Junqiang Wang, Zhijie Li, Sa Zhang, Shengnan Yan, Baobao Cao, Zhiguo Wang, Yongqing Fu

Please cite this article as: Junqiang Wang, Zhijie Li, Sa Zhang, Shengnan Yan, Baobao Cao, Zhiguo Wang, Yongqing Fu, Enhanced NH3 gas-sensing performance of silica modified CeO2 nanostructure based sensors, Sensors and Actuators B: Chemicalhttp://dx.doi.org/10.1016/j.snb.2017.08.149

Enhanced NH₃ gas-sensing performance of silica modified CeO₂ nanostructure based sensors

Junqiang Wang[1], Zhijie Li[1*], Sa Zhang[1], Shengnan Yan[1], Baobao Cao[2], Zhiguo Wang[1], Yongqing Fu[3*]

[1]School of Physical Electronics, University of Electronic Science and Technology of China, Chengdu, 610054, P. R. China

[2]A Key Laboratory of Advanced Technologies of Materials, Ministry of Education, Southwest Jiaotong University, Chengdu 610031, China

[3]Faculty of Engineering and Environment, Northumbria University, Newcastle Upon Tyne, NE1 8ST, UK

Highlights

- The silica modified CeO₂ nanostructures are synthesized using a sol-hydrothermal route and used as NH₃ gas-sensing materials.

- At room temperature, the 8%silica-CeO₂ based gas sensor shows high gas response of 3244% to 80 ppm of NH₃ and lower detection limit (0.5 ppm) towards NH₃ gas.

- The gas response of the NH₃ sensor has good linear characteristics for NH₃ gas detecting.

- The NH₃ sensor exhibits good reproducibility, selectivity and long-term stability to NH₃ gas.

Abstract

The silica modified CeO₂ gas sensing nanomaterials are synthesized using a sol-hydrothermal route. The 8%silica-CeO₂ has larger specific surface areas of 83.75 m²/g and smaller crystalline size of 11.5 nm than pure CeO₂, respectively. Compared to pure CeO₂, the 8%silica-CeO₂ based gas sensor exhibits significant enhancement

1

NH$_3$ gas-sensing performance. At room temperature, it shows much better gas response of 3244% to 80 ppm of NH$_3$ gas and lower detection limit (0.5 ppm) towards NH$_3$ gas. It is also found that the gas response of the NH$_3$ gas sensors increases linearly with the increase of NH$_3$ gas concentration. Moreover, the NH$_3$ gas sensor have good reversibility, stability and selectivity. The reason of enhanced NH$_3$ gas-sensing performance is not only because of the increased specific surface areas, but also due to the electrolytic conductivity of NH$_4^+$ and OH$^-$ on the surface.

Keywords: CeO$_2$; Gas sensor; Silica; Hydrothermal; NH$_3$

1 Introduction

Being one of the major air pollution resources, ammonia gas (NH$_3$) is commonly released from organic nitrogenous animal and vegetable matters, organic decomposition, industrial effluents and motor vehicles [1]. It is also one of the important industrial chemicals, which have been used to make pharmaceuticals, plastics, fertilizers, cleaning products, dyes, explosives and synthetic fibers. However, ammonia is hazardous substance and may cause burns and swelling in the airways, or lung damage, and skin and eye damage. Therefore, an ammonia sensor with high response, good selectivity, long-term stability and low detection limit is critical and urgently needed. So far, various materials have been explored to detect NH$_3$ gas, such as SnO$_2$ [2-5], V$_2$O$_5$ [6], WO$_3$ [7, 8], Co$_3$O$_4$ [9, 10], ZnO [11-13], TiO$_2$ [14], carbon nanotubes [15, 16], graphene [17, 18], etc. However, the gas response using these materials is not high enough, and the detection limit of ammonia is above ppm level. Most of these sensors need to be operated at an elevated working temperature. Therefore, it is still a challenge to design and fabricate new types of gas sensors with a high response to detect sub-ppm level of NH$_3$ at room temperature.

As one of the potential sensing materials for environmental gas monitoring, cerium oxide (CeO$_2$) has advantages of good resistance to chemical corrosion, non-toxicity, safety and reliability. therefore, it have attracted significant attention as gas sensors

for CO [19, 20], H_2S [21], C_2H_5OH [22], and carbon disulfide [23], acetone [24]. Improved gas sensing performance can be further achieved by modifying of structures CeO_2. For example, the gas response of sensors could be significantly increase by incorporation of Pt nanoparticles onto CeO_2 nanowire [19]. Gas sensor based on mixtures of CeO_2-Fe_2O_3 enhanced adsorption and subsequent oxidation of methanol [25]. Core-shell structures of CeO_2/TiO_2 nanorods exhibited enhanced response and selectivity to ethanol vapor [26]. Gas sensor based on CeO_2-ZnO showed improved gas response and selectivity to ethanol than pure CeO_2 sensor [27]. It is well documented that the addition of silica in metal oxides can stabilize the nanocrystal and enhance their catalytic activity [28, 29]. Moreover, according to the paper reported by George et al [30], the silica surface is terminated by lots of hydroxyl groups at the atmospheric pressure and temperatures below $150\,^{\circ}C$, and the hydroxyl groups have extraordinary ability of water absorption [31]. Therefore, at room temperature, ammonia molecules will be adsorbed and react with water molecules on the surface of silica modified CeO_2 to produce NH_4^+ and OH^- ions. The NH_4^+ and OH^- ions will result in a decrease of electric resistance, which will increase the gas response of the sensor. However, the NH_3 gas-sensing property of gas sensor based on silica modified CeO_2 nanomaterials have not reported.

In this work, we report a NH_3 gas sensor based on the silica modified CeO_2 nanostructures with a high gas response and detection limit of sub-ppm level, operated at room temperature. In addition, gas-sensing mechanisms of the gas sensors are also discussed.

2 Experimental

The pure CeO_2 and silica modified CeO_2 nanomaterials were synthesized using a sol-hydrothermal process. Firstly, at $50\ ^{\circ}C$, a certain amount of tetraethoxysilane (TEOS) was added into 60 mL 0.01 mol/L nitric acid (HNO_3) solution. Then, 10 mmol $Ce(NO_3)_3\cdot 6H_2O$ was added under a constant magnetic stirring. Subsequently, 15 mL $NH_3\cdot H_2O$ was dropwise added into the above solution under continuous stirring to form a sol. After stirred at room temperature for 30 min, the sol was

transferred into an autoclave for hydrothermal reaction at 150 $^{\circ}$C for 10 hours. The precipitates from autoclave was washed centrifugally with distilled water for three times and then dried at 70 $^{\circ}$C for 12 hours. Finally, the precipitates were treated at 400 $^{\circ}$C for 1 h in air to obtain the final 8%silica-CeO$_2$ samples. The SiO$_2$ content was defined as SiO$_2$% = $M_{SiO2}/(M_{SiO2}+M_{CeO2})$, where M_{SiO2} and M_{CeO2} were molar quantities of SiO$_2$ and CeO$_2$, respectively. Pure CeO$_2$ was prepared using the same synthesis process without TEOS.

X-ray diffraction (XRD, D/MAX-2500) with Cu Kα radiation was used to characterize the crystalline structures of the samples. Morphologies and sizes of synthesized samples were studied using a high resolution transmission electron microscope (HRTEM, JEM-2100F). The morphologies of film samples were observed using a scanning electron microscope (SEM, Inspect F50, USA) attached with Energy Dispersive Spectrometer (EDS). The chemical compositions of the samples were analyzed using X-ray photoelectron spectroscopy (XPS, Thermo Fisher Scientific,) with Al Kα radiation. The specific surface area was measured by the N$_2$ physisorption apparatus (JW-BK122W, JWGB SCI. TECH.). UV–Vis diffuse reflectance spectra (DRS) was recorded using UV-2550 spectrophotometer (Shimadzu Corporation, Japan). Fourier transform infrared (FT-IR) spectra are recorded on a FT-IR Transmittance spectrometer (FT-IR, Nicolet 6700, USA) in the range of 400-4000 cm^{-1} at room temperature. The element analysis was conducted by Inductive Coupled Plasma Emission Spectrometer (ICP，AtomScan 16, TJA, USA).

3 Results and discussion

3.1 Microstructure analysis

Fig. 1 shows the TEM, HRTEM images and selected area electron diffraction pattern (SAED) of pure CeO$_2$ and 8%silica-modified CeO$_2$. As illustrated in Fig. 1a, the CeO$_2$ is mono-disperse nanoparticles and the crystal diameters are ranged from 11 to 25 nm. From the HRTEM image shown in Fig. 1b, the CeO$_2$ nanoparticles have hexagonal shape and show a well-defined crystalline structure with an lattice spacing of 0.328 nm corresponding to the (111) planes of the CeO$_2$ phase. The concentric

diffraction rings in the SAED pattern (Fig. 1c) can be to (111), (200), (220), (311), (222), (400) and (331) planes of cubic fluorite CeO_2 crystalline structure. The 8%silica-CeO_2 samples show much finer and well-defined nanocrystal (see Fig. 1e) of cubic fluorite CeO_2 crystalline structure (evidenced from the SAED pattern shown in Fig.1f). However, Fig. 1d and Fig. 1e show that their sizes are much smaller than those of the pure CeO_2 nanocrystals. The estimated diameters of 8%silica-CeO_2 crystalline grains are only ranged from 8 to 12 nm. Clearly, the addition of silica can inhibit the growth of CeO_2 crystalline grains effectively.

Fig. 2a shows the SEM image of 8%silica-CeO_2 film. It can be seen that the 8%silica-CeO_2 film is composed of numerous nanoparticles. And the elemental composition of the 8%silica-CeO_2 film was studied by the corresponding EDS spectrum and the result is displayed in Fig. 2b, which confirms that the sample is composed of Ce, Si and O, and the atomic percentage of Ce, Si and O is about 2.1%, 28.4% and 69.5%, meaning that the Si atomic percentage of total metal amount is 6.9%.

The XRD patterns of pure CeO_2 and 8%silica-CeO_2 are shown in Fig. 3. For both samples, it is obvious that the CeO_2 crystallites have formed with their diffraction peaks at 28.6°, 33.2°, 47.5°, 56.4°, 59.1°, 69.4°, 77.0° and 79.1°, corresponding to (111), (200), (220), (311), (222), (400), (331) and (420) of CeO_2, respectively. It is in good agreement with cubic fluorite structure CeO_2 (JCPDS NO. 34-0394) with the lattice constant of a = b = c = 5.411 Å. No other peaks are observed in the XRD patterns, indicating that the all Ce^{3+} have been transformed Ce^{4+}. And there is not any peak of SiO_2 in the XRD spectrum of 8%silica-CeO_2. Therefore, the SiO_2 should be amorphous in 8%silica-CeO_2, which consists with the results reported previously in the literature [32]. For example, Al-Asbahi used the silica to modify titania nanoparticles, it was found that the SiO_2 was amorphous [33]. And in the silica modified SnO_2 nanoparticles, the SiO_2 also was proved to be amorphous [34]. Furthermore, using the ICP analysis, the molar percentage of SiO_2 in 8%silica-CeO_2 is 8.29%, which is almost consistent with the added quantity of SiO_2 during the synthesis process. According to the standard Scherrer equation, the crystals average

sizes for CeO_2 and 8%silica-CeO_2 nanoparticles are 18.1 and 11.5 nm, respectively. This is in agreement to the results from TEM. It is cleared that CeO_2 crystallinity and size are modified after involving silica, and the silica can effectively reduce of CeO_2 crystalline grains. The reason is that the presence of SiO_2 can reduce the chance of CeO_2 nanoparticles aggregating each other to inhibit growth of CeO_2 crystalline grains [33].

The FT-IR spectrum of 8%silica-CeO_2 is shown in Fig. 4. The strong and wide peak at approximate 3428 cm^{-1} is attributed to the stretching vibration of hydroxyl (O-H), and the absorption peak at 1626 cm^{-1} is attributed to the O-H bending vibration mode [35]. Ce–O–Ce vibration appears in the range from 400 to 600 cm^{-1} as the result of condensation reaction [36]. The peaks at 980 cm^{-1} and 854 cm^{-1} correspond to the asymmetric stretching vibration and symmetric stretching of Si–O–Si [35]. Moreover, the peak observed at 936 cm^{-1} should be due to the stretching vibration band of Ce–O–Si bonds [37], which reveals that Si^{4+} is integrated into the surface of CeO_2. Similar chemical bonds (e.g. Ti-O-Si [33] and Sn-O-Si [34]) have been found in silica modified TiO_2 and SnO_2. The formation of these bonds on the surface of metal oxides will inhibit the growth of metal oxides crystalline grains [34, 38].

The XPS spectra of CeO_2 and 8%silica-CeO_2 are shown in Fig. 5. As seen in the two XPS survey spectra (Fig. 5a), binding energies of Ce 3d and O 1s can be identified. In addition, the survey spectra of 8%silica-CeO_2 shows an apparent signal of Si element (see inset spectra in Fig 5a), proving the existence of silicon element in 8%silica-CeO_2. Fig. 5b shows a high resolution spectrum of Si 2p, in which the binding energy located at around 101.4 eV is assigned to Si $2p_{3/2}$ [39], which reveals that Si element existed as valence state of Si(Ⅳ) in the sample. The high resolution Ce 3d spectra of the CeO_2 and 8%silica-CeO_2 are shown in Fig. 5c. It can be seen that the typical six peaks of Ce 3d are generated into three pairs of spin orbit doublets. The binding energy located at around 916.7, 907.5 and 900.8 eV are corresponded to Ce $3d_{3/2}$, and those at 898.2, 888.7 and 882.3 eV are assigned to the Ce $3d_{5/2}$, indicating a normal oxidation valence state of Ce^{4+} in the CeO_2 crystals [40]. The concentrations of various elements in the sample were calculated using the integrated area of each

corresponding peak in the spectrum. The Si atoms percentage composition of total metal amount in 8%silica-CeO_2 nanoparticles is 7.1% and that of the Ce atoms is 92.9%, which almost corresponds to the original atom ratio (8%) in the reaction mixtures.

The high resolution O1s peaks of pure CeO_2 and 8%silica-CeO_2 are shown in Fig. 5d. The binding energies of O1s peaks for pure CeO_2 are 529.0 and 531.2 eV. The lower binding energy of 529.0 eV is corresponding to the oxygen in the crystal lattice of CeO_2. And the higher binding energy of 531.2 eV is attributed to the hydroxyl groups (-OH) on the surface of nanoparticles due to the surface adsorption, which have been reported on the surface of many metal oxides [41]. For the 8%silica-CeO_2, the binding energy attributed to the oxygen in the crystal lattice appeared a chemical shift to 529.3 eV, which should be due to the formation of Ce-O-Si bonds on the surface of CeO_2 [42]. The binding energy attributed to the hydroxyl groups also appears at 531.4 eV. Calculated by the area of each corresponding peak, the hydroxyl group percentage composition in total oxygen on the surface of CeO_2 nanoparticles are 24.5% and 51.1% for pure CeO_2 and 8%silica-CeO_2, respectively. It is clear that, due to the additive of silica [31], there are more hydroxyl groups on the surface of 8%silica-CeO_2 than those on the pure CeO_2.

Using the BET method, the specific surface areas for pure CeO_2, 8%silica-CeO_2 and 14%silica-CeO_2 are 50.57, 83.75 and 90.32 m^2/g respectively. The silica modified CeO_2 have larger surface areas than the pure CeO_2 due to its smaller particles size. The larger surface areas is beneficial to the absorption of target gas molecule in the application of gas sensors.

The UV-Vis DRS spectra of samples are shown in Fig. 6. The absorption edges of CeO_2 and 8%silica-CeO_2 are 379.5 and 374.6 nm respectively, meaning that the band gap is 3.27 and 3.31 eV. So, an obviously blue shift of the absorbing band edge happens with the addition of silica. Because the sizes of 8%silica modified CeO_2 crystals (11.5 nm) is smaller than pure CeO_2 (18.1 nm), the blue shift should be due to the well-known quantum size effect [43].

3.2 Gas sensing properties

The gas sensor was fabricated by coating the samples on the surface of ceramic tube with a pair of gold electrodes. The measurement circuit is connected to the gold electrodes on the ceramic tube using Pt wires. The illustration of NH_3 gas-sensing measurement system is showed in Fig. 7. The details of measurement process of the sensor are similar to those reported in the literature [44]. During the measurement, the working voltage is set as 5 V and the relative humidity is 30%. The gas response of gas-sensing can be defined as following equations:

$$\text{Gas response} = \frac{R_{air} - R_{gas}}{R_{gas}} \times 100\% \qquad (1)$$

where R_{air} and R_{gas} are the sensing material electric resistance in air and target gas, respectively.

The response/recovery curves of the gas sensors made of pure CeO_2 and silica modified CeO_2 were investigated under different concentration of NH_3 gas at room temperature, and the results are summarized in Fig. 8. When the NH_3 gas is injected in the testing chamber, the electric resistance of the sensors decrease remarkably, but it returns to its original reading after the NH_3 gas is pumped. This indicates that the NH_3 gas sensors have a good reversibility. The gas response of pure CeO_2 and silica-CeO_2 based sensors is found to increase with increasing of NH_3 gas concentrations. To investigated the effect on gas response of different silica content, the 14%silica-CeO_2 was also prepared using the same synthesis process, and the response/recovery curves to NH_3 gas of the 14%silica-CeO_2 based gas sensor is also measured and the results are shown in Fig. 8c. Compared with those of the pure CeO_2 and 14%silica-CeO_2, the 8%silica-CeO_2 based gas sensor has the highest gas response and the lowest detection limit towards NH_3 gas. For detecting the 80 ppm of NH_3 gas, the gas response of 8%silica-CeO_2 sensor is 3244%, which is ~6.4 times and ~3.5 times for those of the CeO_2 (508%) and 14%silica-CeO_2 (937%) based gas sensors, respectively. The 8%silica-CeO2 based gas sensor still maintains an evident gas response of 20% toward 0.5 ppm of NH_3 gas. However, when the NH_3 gas concentration is lower than 5 ppm, the gas response of CeO_2 and 14%silica-CeO_2 based sensors are negligible.

8

The detection limits towards NH_3 gas are 10 ppm and 5 ppm for the CeO_2 and 14%silica-CeO_2 based sensors, respectively. Evidently, the modification of silica can remarkably improve the NH_3 gas-sensing performance of CeO_2 based sensing materials. When the content of silica is 8%, the NH_3 gas sensor gets the best gas-sensing performance, which indicates that there is an optimal content of silica with respect to sensor performance. For the lower silica content of 8%, Si^{4+} ions are integrated into the surface of CeO_2 to increase the sensing performance. However, for the higher silica content of 14%, there are more silica nanoparticles in samples. Therefore, although the specific surface area of 14%silica-CeO_2 increase, but the silica nanoparticles would isolate the CeO_2 nanocrystals, which will result that the increase of sensing performance is not significant. [34]

The working temperature, gas response and detection limit are the key parameters for the gas sensor. Among many different types of NH_3 gas sensors reported, the SnO_2-nanowire gas sensors had a response of 300 to 1000 ppm NH_3 gas at a working temperature of 200 °C [5] . NH_3 gas sensors based on hollow NiO–SnO_2 nanospheres showed a good responses to 20 ppm of NH_3 gas at a working temperature of 300 °C and the detected limit was 5 ppm [45]. A nano-crystalline WO_3 layer exhibited the best gas response about 95% to 100 ppm NH_3 at 220°C [7]. The working temperature of these NH_3 gas sensors were above 200°C. The NH_3 gas sensor conducted at the room temperature was also reported. For example, Liu et al. [46] reported that PbS quantum dots/TiO_2 nanotubes arrays showed a gas response of 17.49 for 100 ppm ammonia gas with a detection limit of 2 ppm at room temperature. Li et al. [47] reported that polyaniline/SnO_2 heterojunction had good selectivity to NH_3 gas at room temperature of 21°C, and its detection limit was 1.8 ppm. However, the detection limits of these NH_3 gas sensors was above 1 ppm. The sensing properties of NH_3 gas sensors based different sensing materials reported previously in the literatures were listed in the table 1. It is obviously that the NH_3 gas sensor based on 8%silica-CeO_2 nanoparticles shows the good performance with high response and low detection limit (0.5 ppm) at room temperature.

Fig. 8d shows the gas response of the different sensors as a function of NH_3 gas

9

concentration. It is obvious that the gas response of the pure CeO_2 and silica modified CeO_2 sensors increases linearly with the increase of NH_3 gas concentration. Based on the data, the linear function equation fitted for the NH_3 concentration (C_{NH3}) and the gas response (S) are summarized as follows:

$$S(CeO_2) = 5.9073C_{NH3} + 26.2927 \qquad (R^2 = 0.9923) \qquad (2)$$

$$S(8\%silica\text{-}CeO_2) = 43.1052C_{NH3} + 44.6002 \qquad (R^2 = 0.9910) \qquad (3)$$

$$S(14\%silica\text{-}CeO_2) = 11.4267C_{NH3} + 49.2818 \qquad (R^2 = 0.9758) \qquad (4)$$

where R^2 is fitted relation coefficient. It can be seen that three gas sensors have good linear characteristics for NH_3 gas detecting. The NH_3 gas sensor based on 8%silica-CeO_2 exhibits the largest slope and a wide linear response, meaning that it is more sensitive than CeO_2 and 14%silica-CeO_2 based gas sensors. The good linearity characteristic and high gas response of the 8%silica-CeO_2 sensor at room temperature are advantageous to the practical application of the NH_3 gas senor.

From the above results, the NH_3 gas sensor based on 8%silica-CeO_2 shows high gas response at room temperature. Its response/recovery time and selectivity were further investigated. Fig. 9a shows the response time and recovery time of 8%silica-CeO_2 based gas sensor at different concentration of NH_3 gas at room temperature. The recovery times are decreased with the decreasing of NH_3 gas concentration from 80 to 0.5 ppm. However, the response times are not consistent with the performance of recovery time, Under 3 ppm of NH_3, the response time decrease with the decreasing of NH_3 gas concentration. But above 3 ppm of NH_3, the response times all are about 760 s, except for 60 ppm. For the 0.5 ppm NH_3 gas, the sensor based on the 8%silica-CeO_2 showed fast response, and the response time and recovery time are 32 and 141 s respectively. Fig. 9b displays the response/recovery curves of the sensor is exposed to various gases (H_2, H_2S, C_2H_5OH, CO, NO_2 and NH_3) at the same gas concentration of 80 ppm. There are insignificant response of the gas sensor to H_2, H_2S, C_2H_5OH, CO and NO_2 gases, but with a high gas response of 3244% for NH_3 gas. This is maybe because lots of hydroxyl groups on the 8%silica-CeO_2 nanoparticles will prevent the reaction of other gases on the surface of sensing materials. Therefore, the sensor based on 8%silica-CeO_2 have good selectivity for NH_3 detection.

Fig. 10a shows the dynamic response/recovery curves of sensor based on 8%silica-CeO_2 under higher NH_3 concentration at room temperature. It was found that the response of the sensor tend to constant about 3481% when NH_3 gas concentration is higher than 80 ppm. Therefore, the linear relation between sensing response and NH_3 concentration could not be maintained under higher NH_3 concentration (> 80 ppm NH_3). The humidity influences on the performance of the sensors was tested, and the dynamic response/recovery curves of the sensor to 80 ppm NH_3 gas under different relative humidity at room temperature are displayed in Fig. 10b. It can been seen that the response of the sensor increased with the increase of relative humidity from 30% to 70%. Furthermore, the gas sensor almost have not response in the dry air. This indicated the sensing performance of the NH_3 sensor based on 8%silica-CeO_2 was influenced significantly by the humidity. It can be seen from Fig. 9a that the recovery time of the sensor is long, especially under higher NH_3 concentrations. In order to reduce the recovery time, the heating approach was adopted during recovery process. Fig. 10c shows the dynamic response/recovery curves of the sensor to 40 ppm NH_3 gas at different recovery temperature. It can be found that the recovery time was 1960 s at the room temperature of 25 ℃, but it was only 3s when the temperature was increased to 100 ℃ during recovery process. This means that the recovery time can be significantly reduced by increasing the recovery temperature.

Reproducibility of the gas sensor was characterized by repeatedly exposing it to the NH_3 gas with a concentration of 40 ppm at room temperature into the chamber and then pumping out, and the measurement results are shown in Fig. 11a. During the repeats absorption and desorption of NH_3 gas, the transient response/recovery curves for five cycles are nearly identical, with insignificant fluctuation of electric resistance. This reveals that the 8%silica-CeO_2 based sensor has a good reproducibility. Stability of this gas sensor was also investigated as shown in Fig. 11b. It can be seen that the gas response deviation is <3% after long-term testing in 40 ppm of NH_3 for 30 days, indicating that the sensor based 8%silica-CeO_2 also has a good long-term stability.

3.3 gas sensing mechanism

In NH_3 sensing process, the oxygen molecules absorb on the surface of silica-modified CeO_2 nanoparticles in air and capture electrons from conduction band to form chemisorbed oxygen species, such as O^-, O^{2-} and O_2^- [52], which results in the formation of a depletion region on the surface of the silica-modified CeO_2 nanoparticles. It is well known that the types of absorbed oxygen species are dependent on the working temperature. At room temperatures, O_2^- is commonly chemisorbed on the surfaces of the nanoparticles [21]. When the sensor is exposed to NH_3 gas, some NH_3 gas molecules will be adsorbed on the surface of silica-modified CeO_2 nanoparticles. The reactions between the NH_3 gas molecule and adsorbed oxygen species can be expressed using the following equations [53]:

$$NH_{3(gas)} \rightarrow NH_{3(ads)} \tag{5}$$

$$4\,NH_{3(ads)} + 3O_{2\,(ads)}^- \rightarrow 2N_2 + 6H_2O + 3e^- \tag{6}$$
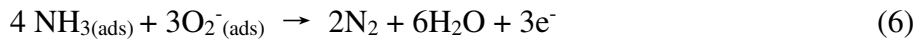
In this progress, the produced electrons will be released into the conduction band of the CeO_2, leading to the reduction of thickness of the election-depletion layer and decreased electric resistance of the sensors. Compared the pure CeO_2, the increased specific surface areas means that there are more chemisorbed oxygen species on the silica-modified CeO_2. Therefore, the silica-modified CeO_2 shows enhanced gas response.

Moreover, XPS analysis have proved that there are lots of hydroxyl groups on the 8%silica-CeO_2 nanoparticles. At room temperature, water molecules will be absorbed on the surface of silica-modified CeO_2 nanoparticles after the sensor is exposed to the ambient air. As we known, ammonia gas has a high solubility, the volume ratio of ammonia could be 700:1 in water. When the NH_3 gas is injected in the testing chamber, some ammonia gas molecules will be adsorbed and react with water molecules on the surface of 8%silica-CeO_2 to produce NH_4^+ and OH^- ions, which can be revealed from as the following reaction:

$$NH_{3(abs)} + H_2O \leftrightarrow NH_4^+ + OH^- \tag{7}$$

The detailed mechanism of reaction is shown in Fig. 12. The electrolytic conductivity of NH_4^+ and OH^- initiates, resulting in a decrease of electric resistance of the sensor. Due to abundant hydroxyl groups on the 8%silica-CeO_2 nanoparticles, lots of H_2O

molecules will be absorbed on the surface and many NH_4^+ and OH^- ions will be formed. Therefore, the formation of NH_4^+ and OH^- are the crucial reason for the high gas response of the 8%silica-CeO_2 based sensors [54]. When the ammonia gas was pumped away and air was injected in the testing chamber, the reaction (7) will become reverse, thus resulting in the resistance of sensor to its original value.

4 Conclusion

In summary, the 8%silica-CeO_2 nanoparticles were synthesized using a sol-hydrothermal route. The addition of silica effectively inhibited the growth of CeO_2 crystals. The 8%silica-CeO_2 had larger specific surface areas and smaller crystal sizes than pure CeO_2. The gas sensor based on 8%silica-CeO_2 nanoparticles showed a higher gas response and a lower detection limit (0.5 ppm) than those of the CeO_2 towards NH_3 gas at room temperature. Furthermore, The NH_3 sensor also showed a good stability and reversibility and a good selectivity to NH_3 gas, indicating that the 8%silica-CeO_2 based gas sensor could be successfully applied in monitoring NH_3 gas.

13

References

[1] X. Li, X. Li, Z. Li, J. Wang, J. Zhang, WS_2 nanoflakes based selective ammonia sensors at room temperature, Sens. Actuators B Chem. 240 (2017) 273-277.

[2] M. Shahabuddin, A. Sharma, J. Kumar, M. Tomar, A. Umar, V. Gupta, Metal clusters activated SnO_2 thin film for low level detection of NH_3 gas, Sens. Actuators B Chem. 194 (2014) 410-418.

[3] K.-Y. Choi, J.-S. Park, K.-B. Park, H.J. Kim, H.-D. Park, S.-D. Kim, Low power micro-gas sensors using mixed SnO_2 nanoparticles and MWCNTs to detect NO_2, NH_3, and xylene gases for ubiquitous sensor network applications, Sens. Actuators B Chem. 150 (2010) 65-72.

[4] B.-H. Jang, O. Landau, S.-J. Choi, J. Shin, A. Rothschild, I.-D. Kim, Selectivity enhancement of SnO_2 nanofiber gas sensors by functionalization with Pt nanocatalysts and manipulation of the operation temperature, Sens. Actuators B Chem. 188 (2013) 156-168.

[5] L.V. Thong, N.D. Hoa, D.T.T. Le, D.T. Viet, P.D. Tam, A.-T. Le, N.V. Hieu, On-chip fabrication of SnO_2-nanowire gas sensor: The effect of growth time on sensor performance, Sens. Actuators B Chem. 146 (2010) 361-367.

[6] V. Modafferi, G. Panzera, A. Donato, P.L. Antonucci, C. Cannilla, N. Donato, D. Spadaro, G. Neri, Highly sensitive ammonia resistive sensor based on electrospun V_2O_5 fibers, Sens. Actuators B Chem. 163 (2012) 61-68.

[7] M. Takács, C. Dücső, A.E. Pap, Fine-tuning of gas sensitivity by modification of nano-crystalline WO_3 layer morphology, Sens. Actuators B Chem. 221 (2015) 281-289.

[8] Y. Wang, J. Liu, X. Cui, Y. Gao, J. Ma, Y. Sun, P. Sun, F. Liu, X. Liang, T. Zhang, G. Lu, NH_3 gas sensing performance enhanced by Pt-loaded on mesoporous WO_3, Sens. Actuators B Chem. 238 (2017) 473-481.

[9] J. Deng, R. Zhang, L. Wang, Z. Lou, T. Zhang, Enhanced sensing performance of the Co_3O_4 hierarchical nanorods to NH_3 gas, Sens. Actuators B Chem. 209 (2015) 449-455.

[10] Z. Li, Z. Lin, N. Wang, J. Wang, W. Liu, K. Sun, Y.Q. Fu, Z. Wang, High precision NH_3 sensing using network nano-sheet Co_3O_4 arrays based sensor at room temperature, Sens. Actuators B Chem, 235 (2016) 222-231.

[11] G.N. Dar, A. Umar, S.A. Zaidi, S. Baskoutas, S.W. Hwang, M. Abaker, A. Al-Hajry, S.A. Al-Sayari, Ultra-high sensitive ammonia chemical sensor based on ZnO nanopencils, Talanta. 89 (2012) 155-161.

[12] V.B. Raj, A.T. Nimal, Y. Parmar, M.U. Sharma, K. Sreenivas, V. Gupta, Cross-sensitivity and selectivity studies on ZnO surface acoustic wave ammonia sensor, Sens. Actuators B Chem. 147 (2010) 517-524.

[13] S. Anantachaisilp, S.M. Smith, C. Ton-That, T. Osotchan, A.R. Moon, M.R. Phillips, Tailoring Deep Level Surface Defects in ZnO Nanorods for High Sensitivity Ammonia Gas Sensing, J. Phys. Chem. C. 118 (2014) 27150-27156.

[14] W. Meng, L. Dai, W. Meng, H. Zhou, Y. Li, Z. He, L. Wang, Mixed-potential type NH_3 sensor based on TiO_2 sensing electrode with a phase transformation effect, Sens. Actuators B Chem. 240 (2017) 962-970.

[15] T. Zhang, M.B. Nix, B.-Y. Yoo, M.A. Deshusses, N.V. Myung, Electrochemically Functionalized Single-Walled Carbon Nanotube Gas Sensor, Electroanal. 18 (2006) 1153-1158.

[16] J.-W. Han, B. Kim, J. Li, M. Meyyappan, A carbon nanotube based ammonia sensor on cotton textile, Appl. Phys. Lett. 102 (2013) 193104.

[17] N. Hu, Z. Yang, Y. Wang, L. Zhang, X. Huang, H. Wei, L. Wei, Y. Zhang, Ultrafast and sensitive room temperature NH3 gas sensors based on chemically reduced graphene oxide, Nanotechnology. 25 (2014) 025502.

[18] M. Gautam, A.H. Jayatissa, Graphene based field effect transistor for the detection of ammonia, J. Appl. Phys. 112 (2012) 064304.

[19] L. Liao, H.X. Mai, Q. Yuan, H.B. Lu, J.C. Li, C. Liu, C.H. Yan, Z.X. Shen, T. Yu, Single CeO_2 Nanowire Gas Sensor Supported with Pt Nanocrystals: Gas Sensitivity, Surface Bond States, and Chemical Mechanism, J. Phys. Chem. C. 112 (2008) 9061-9065.

[20] P. Chesler, C. Hornoiu, V. Bratan, C. Munteanu, G. Postole, N.I. Ionescu, T.

Juzsakova, A. Redey, M. Gartner, CO sensing properties of SnO_2–CeO_2 mixed oxides, React. Kinet. Mech. Cata. 117 (2015) 551-563.

[21] Z. Li, X. Niu, Z. Lin, N. Wang, H. Shen, W. Liu, K. Sun, Y.Q. Fu, Z. Wang, Hydrothermally synthesized CeO_2 nanowires for H_2S sensing at room temperature, J. Alloys compd. 682 (2016) 647-653.

[22] J. Liu, M. Dai, T. Wang, P. Sun, X. Liang, G. Lu, K. Shimanoe, N. Yamazoe, Enhanced Gas Sensing Properties of SnO_2 Hollow Spheres Decorated with CeO_2 Nanoparticles Heterostructure Composite Materials, ACS Appl. Mater. Inter. 8 (2016) 6669-6677.

[23] Y. Xuan, J. Hu, K. Xu, X. Hou, Y. Lv, Development of sensitive carbon disulfide sensor by using its cataluminescence on nanosized-CeO_2, Sens. Actuators B Chem. 136 (2009) 218-223.

[24] R. Bene, I.V. Perczel, F. Reti, F.A. Meyer, M. Fleisher, H. Meixner, Chemical reactions in the detection of acetone and NO by a CeO_2 thin film, Sens. Actuators B Chem, 71 (2000) 36-41.

[25] G. Neri, A. Bonavita, G. Rizzo, S. Galvagno, S. Capone, P. Siciliano, Methanol gas-sensing properties of CeO_2–Fe_2O_3 thin films, Sens. Actuators B Chem. 114 (2006) 687-695.

[26] Y.-J. Chen, G. Xiao, T.-S. Wang, F. Zhang, Y. Ma, P. Gao, C.-L. Zhu, E. Zhang, Z. Xu, Q.-h. Li, Synthesis and enhanced gas sensing properties of crystalline CeO_2/TiO_2 core/shell nanorods, Sens. Actuators B Chem. 156 (2011) 867-874.

[27] S. Yan, S. Ma, X. Xu, Y. Lu, H. Bian, X. Liang, W. Jin, H. Yang, Synthesis and gas sensing application of porous CeO_2-ZnO hollow fibers using cotton as biotemplates, Mater. Lett. 165 (2016) 9-13.

[28] F.H. Saboor, A.A. Khodadadi, Y. Mortazavi, M. Asgari, Microemulsion synthesized silica/ZnO stable core/shell sensors highly selective to ethanol with minimum sensitivity to humidity, Sens. Actuators B Chem. 238 (2017) 1070-1083.

[29] G. Aguila, S. Guerrero, P. Araya, Effect of the preparation method and calcination temperature on the oxidation activity of CO at low temperature on CuO-CeO_2/SiO_2 catalysts, Appl. Catal. A-Gen. 462 (2013) 56-63.

[30] O. Sneh, S.M. George, Thermal-stability of hydroxyl-groups on a well-defined silica surface, J. Phys. Chem. 99 (1995) 4639-4647.

[31] B.J. Meulendyk, M.C. Wheeler, M.P. da Cunha, Hydrogen Fluoride Gas Detection Mechanism on Quartz Using SAW Sensors, IEEE Sens. J. 11 (2011) 1768-1775.

[32] A.T. Güntner, M. Righettoni, S.E. Pratsinis, Selective sensing of NH_3 by Si-doped α-MoO_3 for breath analysis, Sens. Actuators B Chem. 223 (2016) 266-273.

[33] B.A. Al-Asbahi, Influence of anatase titania nanoparticles content on optical and structural properties of amorphous silica, Mater. Res. Bull. 89 (2017) 286-291.

[34] A. Tricoli, M. Graf, S.E. Pratsinis, Optimal Doping for Enhanced SnO_2 Sensitivity and Thermal Stability, Adv. Funct. Mater. 18 (2008) 1969-1976.

[35] I.A. Siddiquey, T. Furusawa, Y.-i. Hoshi, E. Ukaji, F. Kurayama, M. Sato, N. Suzuki, Silica coating of CeO_2 nanoparticles by a fast microwave irradiation method, Appl. Surf. Sci. 255 (2008) 2419-2424.

[36] S. Kumar, A.K. Ojha, Ni, Co and Ni-Co codoping induced modification in shape, optical band gap and enhanced photocatalytic activity of CeO_2 nanostructures for photodegradation of methylene blue dye under visible light irradiation, RSC Adv. 6 (2016) 8651-8660.

[37] A.İ. VaİZoĞUllari, A. Balci, İ. Kula, M. UĞUrlu, Preparation, characterization, and adsorption studies of core@shell SiO_2@CeO_2 nanoparticles: a new candidate to remove Hg(II) from aqueous solutions, Turk. J. Chem. 40 (2016) 565-575.

[38] V.V.S. Kumar, Effect of 750keV Argon ion irradiation on nc ZnO-SiO_x thin films, Appl. Surf. Sci. 351 (2015) 819-823.

[39] Y.-J. Lee, H.-J. Ahn, Fabrication of uniform SnO_2-SiO_2-Pt composite nanofibres via co-electrospinning, Ceram. Int. 39 (2013) 5303-5308.

[40] A.Q. Wang, P. Punchaipetch, R.M. Wallace, T.D. Golden, X-ray photoelectron spectroscopy study of electrodeposited nanostructured CeO_2 films, J. Vac. Sci. Technol. B. 21 (2003) 1169.

[41] S. Zhang, P. Song, J. Zhang, H. Yan, J. Li, Z. Yang, Q. Wang, Highly sensitive detection of acetone using mesoporous In_2O_3 nanospheres decorated with Au

nanoparticles, Sens. Actuators B Chem. 242 (2017) 983-993.

[42] S. Phanichphant, A. Nakaruk, D. Channei, Photocatalytic activity of the binary composite CeO_2 /SiO_2 for degradation of dye, Appl. Surf. Sci. 387 (2016) 214-220.

[43] S. Phoka, P. Laokul, E. Swatsitang, V. Promarak, S. Seraphin, S. Maensiri, Synthesis, structural and optical properties of CeO_2 nanoparticles synthesized by a simple polyvinyl pyrrolidone (PVP) solution route, Mater. Chem. Phys. 115 (2009) 423-428.

[44] Z. Li, Y. Huang, S. Zhang, W. Chen, Z. Kuang, D. Ao, W. Liu, Y. Fu, A fast response & recovery H_2S gas sensor based on alpha-Fe_2O_3 nanoparticles with ppb level detection limit, J. Hazard. Mater. 300 (2015) 167-174.

[45] L. Wang, J. Deng, T. Fei, T. Zhang, Template-free synthesized hollow NiO–SnO_2 nanospheres with high gas-sensing performance, Sens. Actuators B Chem. 164 (2012) 90-95.

[46] Y. Liu, L. Wang, H. Wang, M. Xiong, T. Yang, G.S. Zakharova, Highly sensitive and selective ammonia gas sensors based on PbS quantum dots/TiO_2 nanotube arrays at room temperature, Sens. Actuators B Chem. 236 (2016) 529-536.

[47] S. Bai, Y. Tian, M. Cui, J. Sun, Y. Tian, R. Luo, A. Chen, D. Li, Polyaniline@SnO_2 heterojunction loading on flexible PET thin film for detection of NH3 at room temperature, Sens. Actuators B Chem. 226 (2016) 540-547.

[48] L. Wang, Z. Lou, T. Fei, T. Zhang, Templating synthesis of ZnO hollow nanospheres loaded with Au nanoparticles and their enhanced gas sensing properties, J. Mater. Chem. 22 (2012) 4767.

[49] D.J. Late, T. Doneux, M. Bougouma, Single-layer $MoSe_2$ based NH_3 gas sensor, Appl. Phys. Lett. 105 (2014) 233103.

[50] H. Jiang, L. Zhao, L. Gai, L. Ma, Y. Ma, M. Li, Hierarchical rh-In_2O_3 crystals derived from InOOH counterparts and their sensitivity to ammonia gas, CrystEngComm. 15 (2013) 7003.

[51] Y. Zeng, Z. Lou, L. Wang, B. Zou, T. Zhang, W. Zheng, G. Zou, Enhanced ammonia sensing performances of Pd-sensitized flowerlike ZnO nanostructure, Sens. Actuators B Chem. 156 (2011) 395-400.

[52] Y. Huang, W. Chen, S. Zhang, Z. Kuang, D. Ao, N.R. Alkurd, W. Zhou, W. Liu, W. Shen, Z. Li, A high performance hydrogen sulfide gas sensor based on porous α-Fe_2O_3 operates at room-temperature, Appl. Surf. Sci. 351 (2015) 1025-1033.

[53] J.-M. Tulliani, A. Cavalieri, S. Musso, E. Sardella, F. Geobaldo, Room temperature ammonia sensors based on zinc oxide and functionalized graphite and multi-walled carbon nanotubes, Sens. Actuators B Chem. 152 (2011) 144-154.

[54] Z. Li, N. Wang, Z. Lin, J. Wang, W. Liu, K. Sun, Y.Q. Fu, Z. Wang, Room-Temperature High-Performance H_2S Sensor Based on Porous CuO Nanosheets Prepared by Hydrothermal Method, ACS Appl. Mater. Inter. 8 (2016) 20962-20968.

Biographies

Junqiang Wang obtained his B.S. degree at Yancheng Teachers University in 2015. He is a graduate student in School of Physical Electronics at University of Electronic Science and Technology of China. His research interests include applications of nanomaterials and functional thin films for sensors.

Dr. ZhiJie Li is an associate professor in School of Physical Electronics at University of Electronic Science and Technology of China. He obtained his Ph.D degree of physical chemistry from Institute of Coal Chemistry, Chinese Academy of Sciences in 2005. His research interests include nano materials, gas sensors and surface acoustic wave (SAW) devices.

Sa Zhang obtained his B.S. degree at Zhengzhou Normal University in 2015. She is a graduate student in School of Physical Electronics at University of Electronic Science and Technology of China. Her research interests include computer modeling of the electronic structures and radiation effects with density functional theory (DFT) simulation.

Shengnan Yan obtained his B.S. degree at Zhengzhou University of Aeronautics in 2016. She is a graduate student in School of Physical Electronics at University of Electronic Science and Technology of China. Her research interests include applications of nanomaterials and functional thin films for sensors.

Dr. Baobao Cao is an associate professor in School of materials science and Engineering at Southwest Jiao Tong University. He obtained his Ph.D degree of Beijing Key Laboratory of electron microscopy, Institute of physics, Chinese Academy of Sciences in 2008. His research interests include design and controllable preparation of functional nanomaterials and application of transmission electron microscopy in the characterization of fine materials

Dr. Zhiguo Wang is a professor at the University of Electronic Science and Technology of China (UESTC). He graduated from Sichuan University in China and received M.S. in condensed matter physics. He got his Ph.D. in materials physics and chemistry from UESTC. His research interests include computer modeling of the electronic, thermal, mechanical, defect and doping properties of semiconductor,

electrode materials, and radiation detection materials with density functional theory (DFT) simulation, molecular dynamics (MD), DFTMD, and Monte Carlo simulation.

Dr. Yong Qing Fu (Richard) is a Reader in Faculty of Engineering and Environment, University of Northumbria at Newcastle, UK. He was a senior lecturer/Reader inThin Film Centre and Physics Department in University of West of Scotland, UK, and a lecturer in Heriot-Watt University, UK. He obtained his Ph.D degree from Nanyang Technological University, Singapore in 1999, and then worked as a Research Fellow in Singapore-Massachusetts Institute of Technology Alliance, and a Research Associate in University of Cambridge. He has extensive experience in advanced thin film materials, biomedical microdevices, lab-on-chip, micromechanics, microelectrome-chanical systems (MEMS), sensors and microfluidics, shape memory/piezoelectric thin films and nanotechnology.

Figure captions

Fig. 1. (a) TEM image, (b) HRTEM image and (c) the selected area electron diffraction pattern (SAED) of pure CeO_2; (d) TEM image, (e) HRTEM image and (f) SAED of 8%silica-CeO_2.

Fig. 2. (a) SEM image and (b) EDS pattern of 8%silica-CeO_2 film

Fig. 3. X-ray diffraction patterns of CeO_2 and 8%silica-CeO_2.

Fig. 4. FT-IR spectrum of the 8%silica-CeO_2.

Fig. 5. (a) XPS survey spectra of CeO_2 and 8%silica-CeO_2, (b) high resolution binding energy spectra of Si 2p, (c)-(d) high resolution binding energy spectra of Ce 3d, O 1s, respectively.

Fig. 6. UV−Vis diffuse reflectance spectra (DRS) of CeO_2 and 8%silica-CeO_2

Fig. 7. Illustration of gas-sensing measurement system for NH_3 sensors.

Fig. 8. Transient response/recovery curves of samples of sensor towards different concentration of NH_3 gas at room temperature: (a) CeO_2 based sensor, (b) 8%silica-CeO_2 based sensor, (c) 14%silica-CeO_2 based sensor, (d) Variation of the gas response as a function of different concentration NH_3 gas.

Fig. 9. (a) Response/recovery time for different NH_3 concentration; (b) Response/recovery curves to different gases (H_2, H_2S, C_2H_5OH, CO, NO_2 and NH_3 of 80 ppm) of the sensor based on 8%silica-CeO_2 nanoparticles at room temperature.

Fig. 10. Dynamic response/recovery curves of the sensor based on 8%silica-CeO_2: (a) under high NH_3 concentration from 80 to 140 ppm at room temperature; (b) under different relative humidity for 80 ppm NH_3 gas at room temperature; (c) under different recovery temperature for 40 ppm NH_3 gas.

Fig. 11. (a) Reproducibility 40 ppm NH_3 gas and (b) Stability to 40 ppm NH_3 gas of the sensor based on 8%silica-CeO_2 nanoparticles at room temperature.

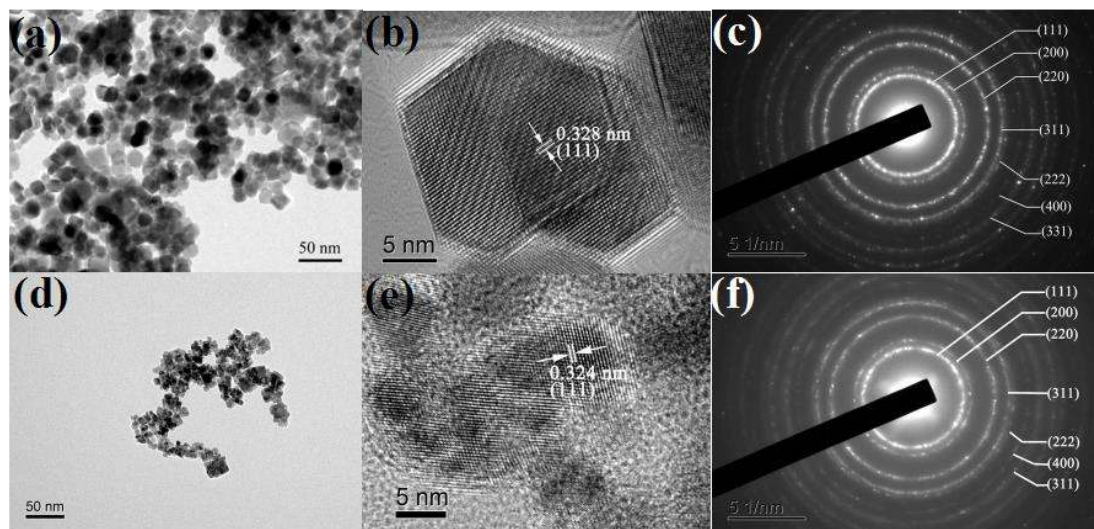Fig. 12. Illustrate of reaction process of mechanism between NH_3 and H_2O molecules.
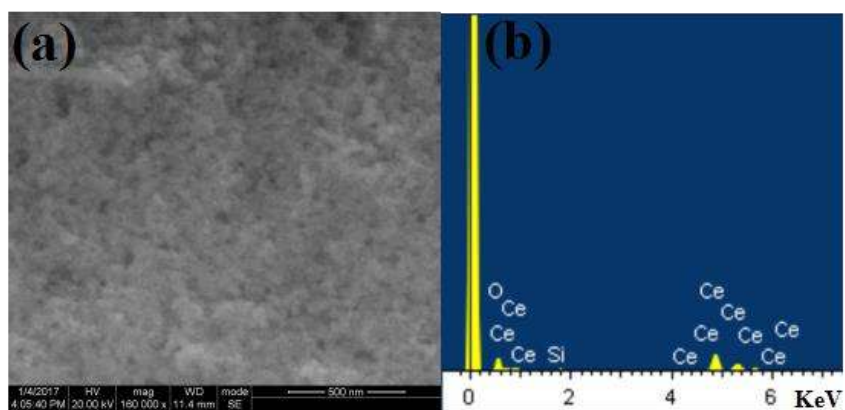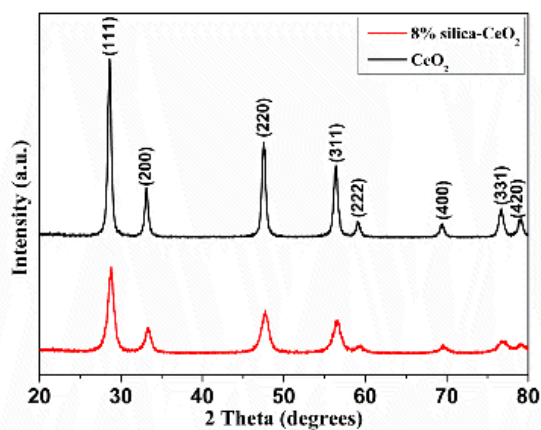
Figure 1

Figure 2

Figure 3

Figure 4
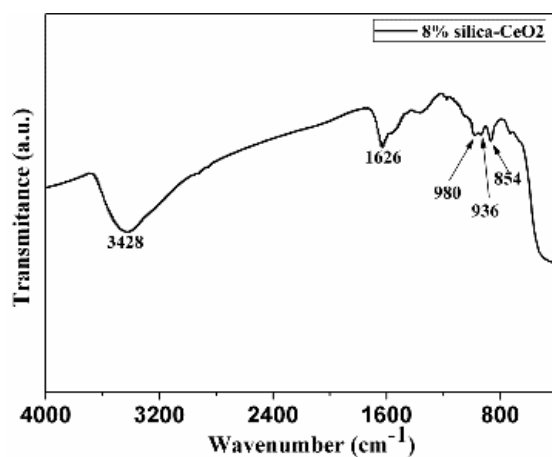
Figure 5
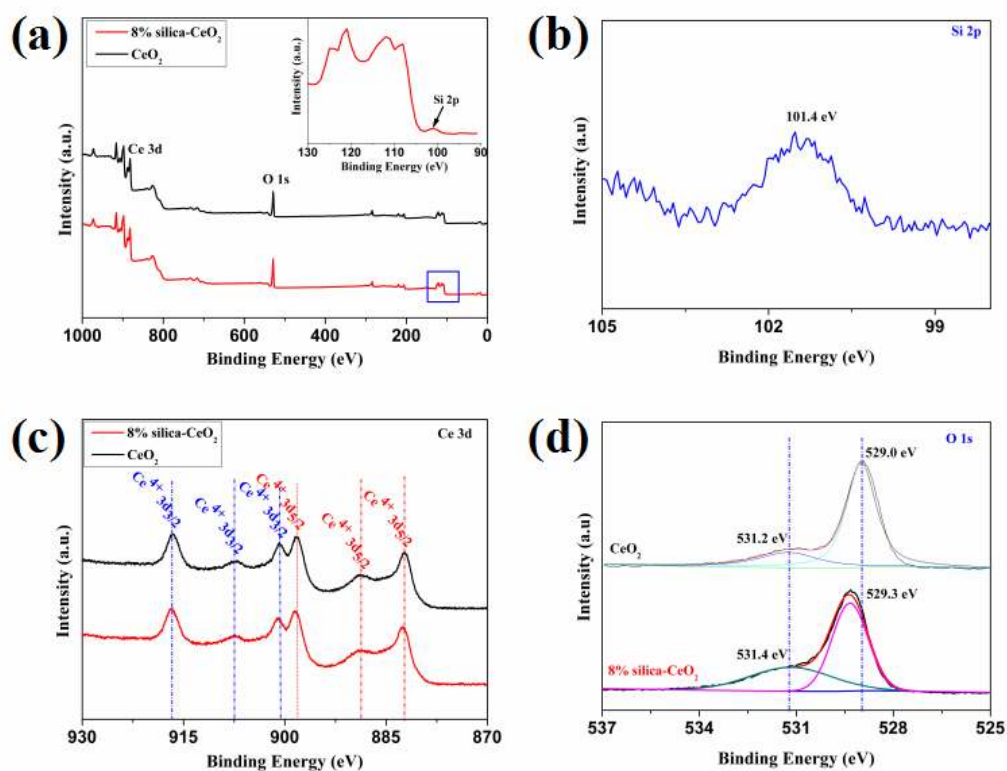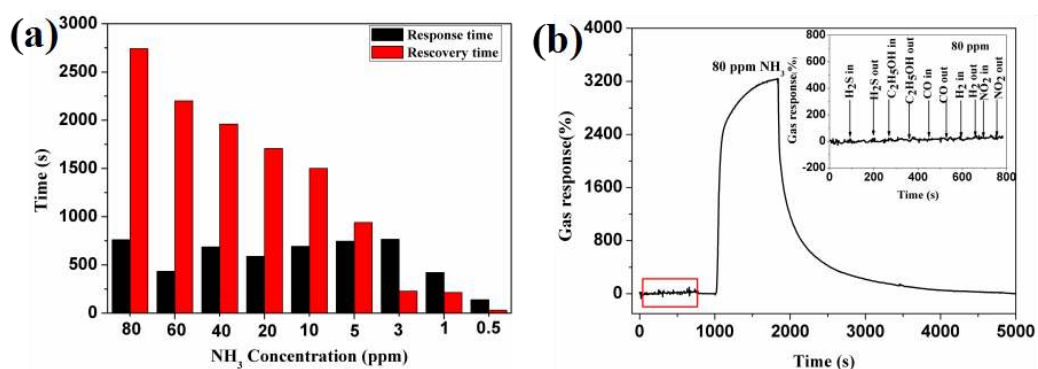
Figure 6
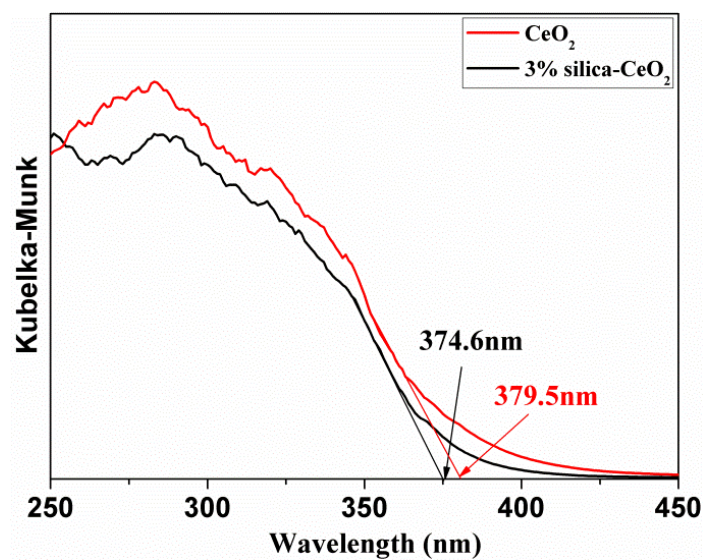
Figure 7
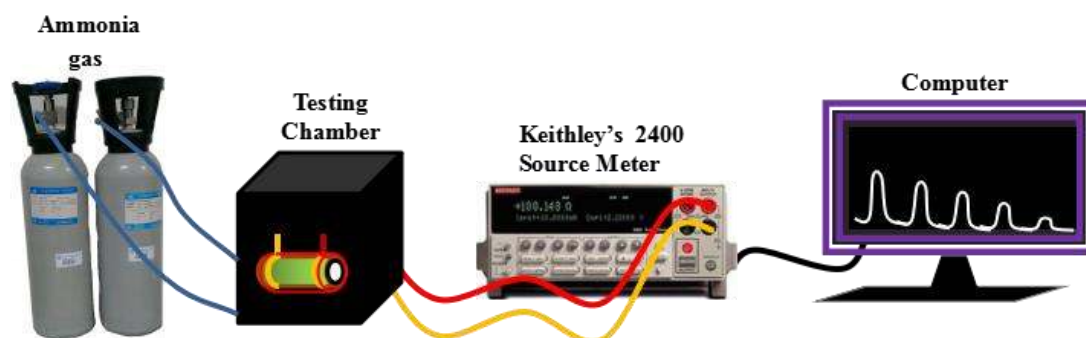
Figure 8
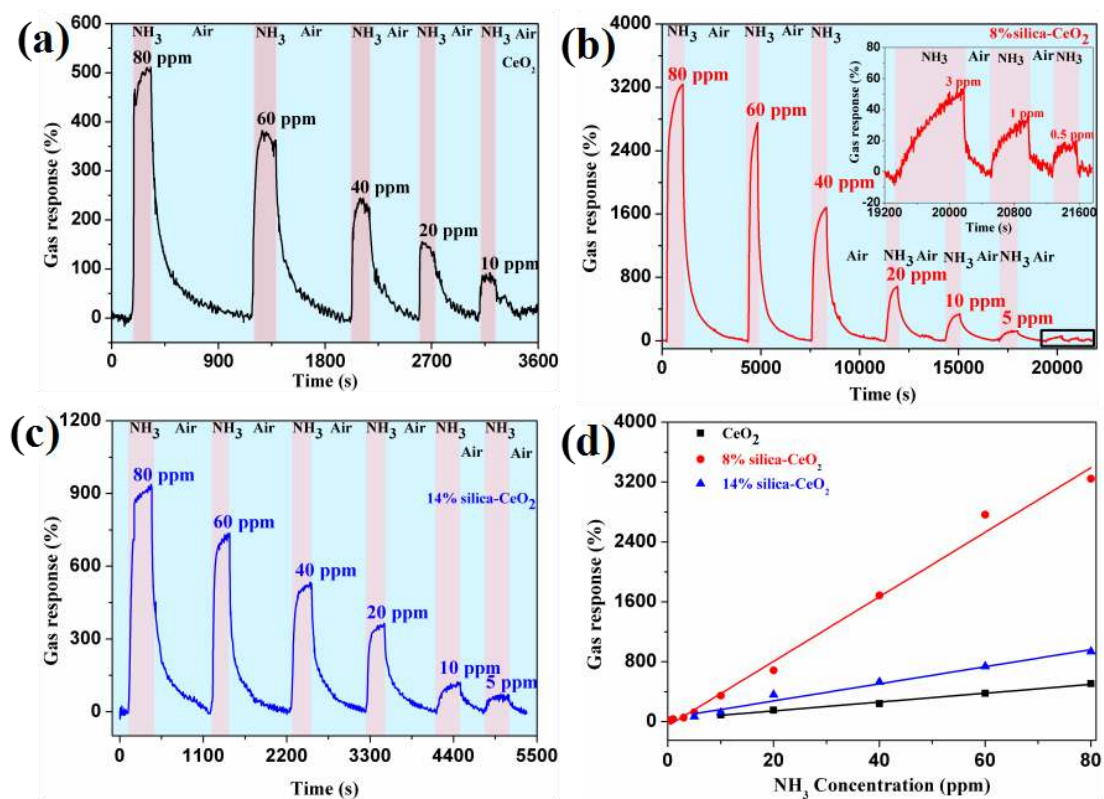
Figure 9

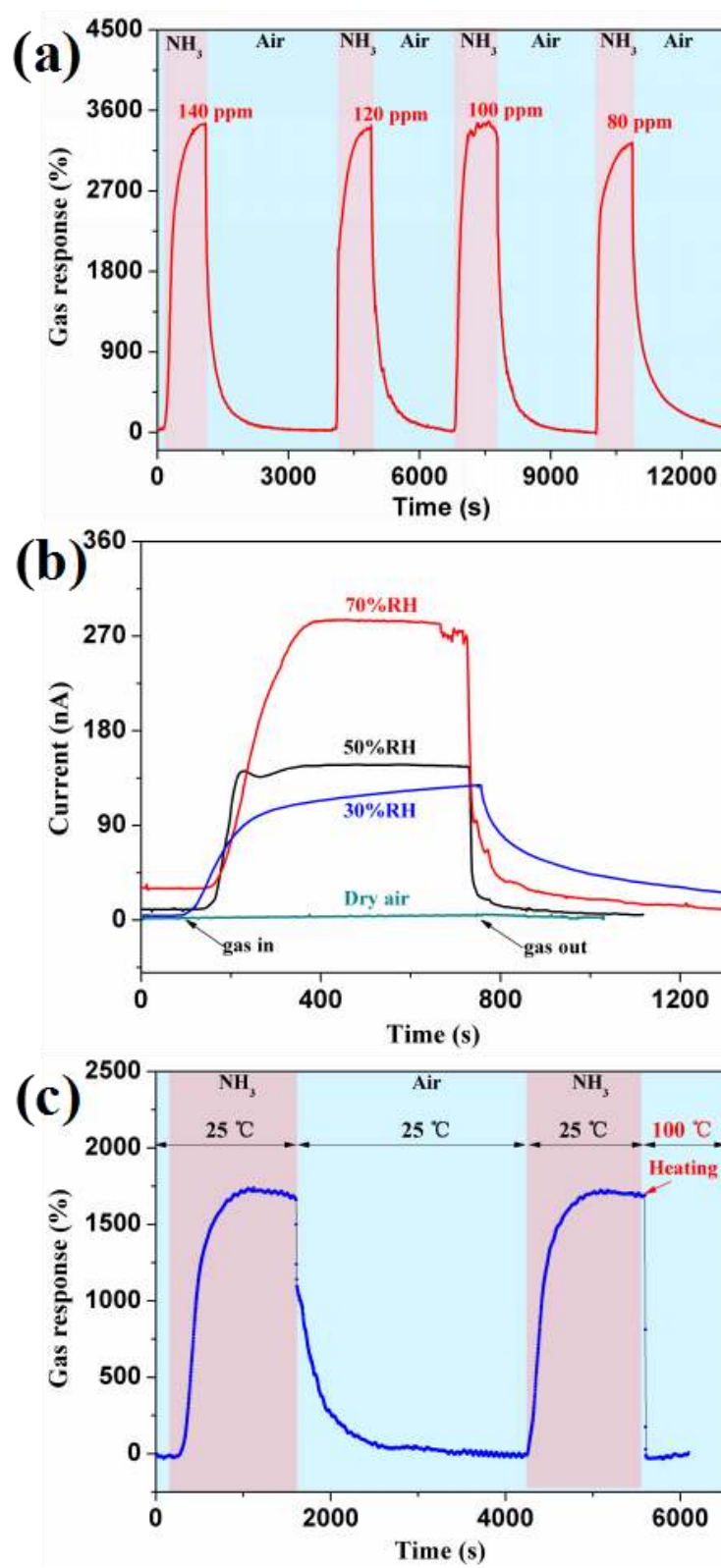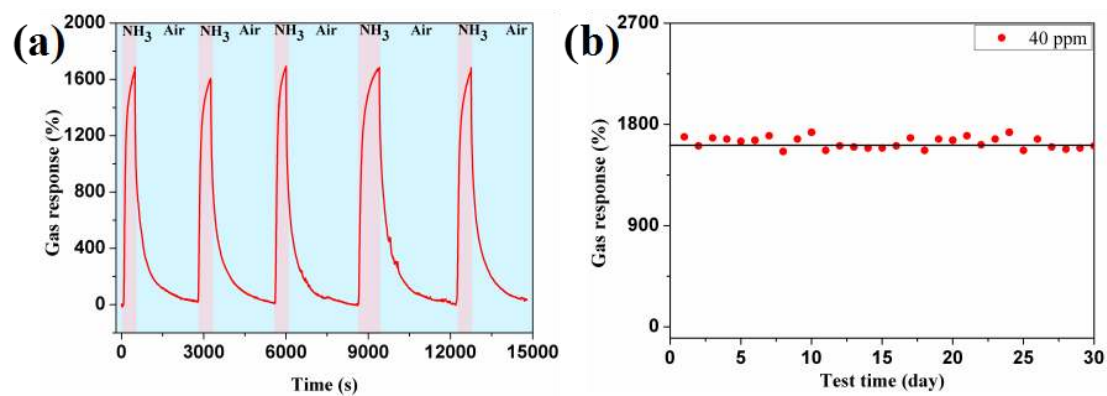**Figure 10**
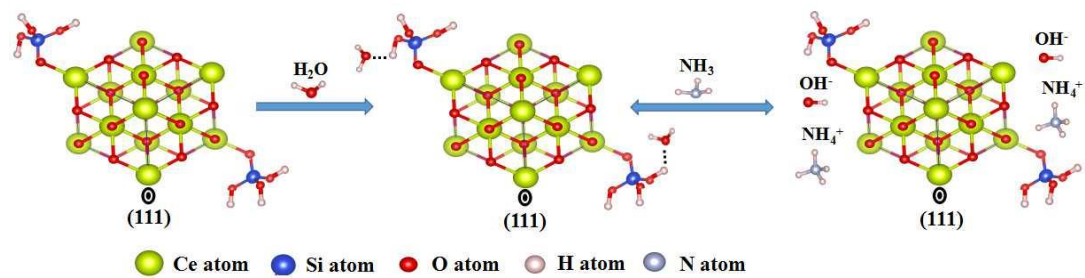
Figure 11

Figure 12

Table 1. The sensing properties of NH_3 gas sensors based different sensing materials.

Sensors	Gas response	Detection limit (ppm)	Working temperature	Ref.
SnO_2	9 (to 300 ppm)	300	200 $^{\circ}$C	[5]
ZnO	9 (to 50 ppm)	5	300 $^{\circ}$C	[48]
WO_3	95% (to 80 ppm)	10	220 $^{\circ}$C	[7]
Co_3O_4	16.3 (to 200 ppm)	10	160 $^{\circ}$C	[9]
$MoSe_2$	1150% (to 500 ppm)	50	25 $^{\circ}$C	[49]
rh-In_2O_3	1.7 (to 5 ppm)	5	300 $^{\circ}$C	[50]
Pd-ZnO	85 (to 100 ppm)	5	210 $^{\circ}$C	[51]
PANI@SnO_2	26 (to 80 ppm)	1.8	25 $^{\circ}$C	[47]
PbS /TiO_2	13 (to 100 ppm)	2	25 $^{\circ}$C	[46]
NiO–SnO_2	60 (to 100 ppm)	5	300 $^{\circ}$C	[45]
CeO_2	508% (to 80 ppm)	5	25 $^{\circ}$C	This work
14%silica-CeO_2	937% (to 80 ppm)	5	25 $^{\circ}$C	This work
8%silica-CeO_2	3244% (to 80 ppm)	0.5	25 $^{\circ}$C	This work